

REPORT DOCUMENTATION PAGE

Form Approved
OMB No. 0704-0188

Public reporting burden for this collection of information is estimated to average 1 hour per response, including the time for reviewing instructions, searching existing data sources, gathering and maintaining the data needed, and completing and reviewing this collection of information. Send comments regarding this burden estimate or any other aspect of this collection of information, including suggestions for reducing this burden to Department of Defense, Washington Headquarters Services, Directorate for Information Operations and Reports (0704-0188), 1215 Jefferson Davis Highway, Suite 1204, Arlington, VA 22202-4302. Respondents should be aware that notwithstanding any other provision of law, no person shall be subject to any penalty for failing to comply with a collection of information if it does not display a currently valid OMB control number. **PLEASE DO NOT RETURN YOUR FORM TO THE ABOVE ADDRESS.**

1. REPORT DATE (DD-MM-YYYY)		2. REPORT TYPE	3. DATES COVERED (From - To)		
4. TITLE AND SUBTITLE			5a. CONTRACT NUMBER		
			5b. GRANT NUMBER		
			5c. PROGRAM ELEMENT NUMBER		
6. AUTHOR(S)			5d. PROJECT NUMBER		
			5e. TASK NUMBER		
			5f. WORK UNIT NUMBER		
7. PERFORMING ORGANIZATION NAME(S) AND ADDRESS(ES)			8. PERFORMING ORGANIZATION REPORT NUMBER		
9. SPONSORING / MONITORING AGENCY NAME(S) AND ADDRESS(ES)			10. SPONSOR/MONITOR'S ACRONYM(S)		
			11. SPONSOR/MONITOR'S REPORT NUMBER(S)		
12. DISTRIBUTION / AVAILABILITY STATEMENT					
13. SUPPLEMENTARY NOTES					
14. ABSTRACT					
15. SUBJECT TERMS					
16. SECURITY CLASSIFICATION OF:			17. LIMITATION OF ABSTRACT	18. NUMBER OF PAGES	19a. NAME OF RESPONSIBLE PERSON
a. REPORT	b. ABSTRACT	c. THIS PAGE			19b. TELEPHONE NUMBER (include area code)

Multiscale Modeling of Stiffness, Friction and Adhesion in Mechanical Contacts FA9550-0910232, Mark O. Robbins, Johns Hopkins University

The mechanical behavior of contacts plays a critical role in the function of devices from aircraft engines to microelectromechanical systems (MEMS). As the demands for performance from these devices increase or their size shrinks, traditional continuum models of contact behavior become inadequate. Overcoming these limitations will require improved understanding of interconnected processes on a wide range of scales from atomic interactions at interfaces to surface roughness on nanometer to micrometer scales and to deformation and loading at macroscopic scales.

One objective of the proposed research was to develop and extend multiscale modeling methods that are capable of bridging between atomistic and continuum models. The first part of this report describes a Green's function method that allowed us to extend the scale of simulations from $\sim 100\text{nm}$ to $\sim 3\mu\text{m}$.

The second objective was to use these multiscale methods to improve understanding of aspects of contact mechanics that are important to Air Force applications. For example, the mechanical behavior of complex assemblies such as gas turbines is strongly influenced by the stiffness of mechanical joints and the dissipation associated with partial slip in these joints. At the other extreme of length scales, MEMS devices often fail due to undesired adhesion that is affected by surface roughness and interfacial forces. Energy loss due to friction forces is important to devices at all scales.

The second section of the report describes studies of single asperity contacts that test the applicability and limits of commonly used continuum descriptions. One study showed that adsorbed monolayers present on most surfaces have a profound impact on contact properties. A second showed that thermal fluctuations lead to normal pressures that are comparable to the ideal yield stress. This makes it difficult to extend continuum definitions of contact to atomic scales. The third study looked for partial slip in contacts with tips up to $2\mu\text{m}$ in radius. The partial slip predicted by continuum models for these scales was not seen. However a simple scaling law was discovered for an unexpectedly strong size dependence in the coefficient of friction.

The third section of the report describes studies of multi-asperity contacts. The contact correlation function for the commonly used bearing area model was obtained and shown to disagree with numerical calculations. Extensive calculations of the stiffness of multiasperity contacts were used to test a simple scaling relation that depends on a few experimental parameters. Finally, a new theory of adhesive contact between rough surfaces was developed that can capture the changes in contact area with load, adhesion strength and other parameters.

The report concludes with a list of papers published and in preparation, and a list of talks on funded research.

1. ALGORITHMIC DEVELOPMENT

A great challenge to tribological studies is that the response is determined by physics on a wide range of length scales. Friction and adhesion forces result from interactions between atoms on opposing surfaces. An accurate model must include the explicit geometry of these atoms. On the other hand, the separation between atoms is controlled by the elasto-plastic response below the surface. To correctly capture subsurface effects, one must include the response to depths D

that are comparable to the lateral extent along the surface L . Meeting both these criteria in a single calculation presents great computational challenges.

Our current fully atomistic simulations of contact are limited to linear dimensions less than 100nm. The corresponding number of atoms is up to 50 million, and calculations take days on a hundred processor cores. Part of the proposal was to search for algorithms that allowed much larger systems to be studied. The key idea is that subsurface deformations vary slowly and may be modeled with more efficient coarse-grained methods.

The method that we found most effective was a generalization of the Green's function approach of Campana and Muser (2006) that was implemented into the molecular dynamics code LAMMPS by Kong et al. (2009). Atoms above some plane are treated fully atomistically. The linear elastic response of atoms below this plane is fully captured using a lattice Green's function. The method is fast because the Green's function is sparse in reciprocal space. A 2D fast Fourier transform (FFT) of atomic displacements in the plane is performed. Forces can then be calculated by multiplying by a precalculated Greens function for each wave vector q and performing an FFT back to real space. The Greens function at each q is a matrix of dimension $3n$ where n is the number of layers that interact with the atomistic region (typically 1-3). The total time scales as $L^2 \ln L$ instead of L^3 .

Our implementation of the method differs in several important ways. One corrects an error that we discovered in the algorithm. When interactions extend beyond the nearest layer of atoms, previous implementations did not correctly treat the change in interactions due to the change in layer spacing. This can be a significant effect in certain cases. We also developed an analytic method for calculating the Greens function at low temperatures. The previous implementation used separate simulations to find G . The final improvement was to implement the algorithm on graphics processor units (GPUs). This allowed us to treat L as large as 8192 atoms or total volumes of 550 trillion atoms on a single GPU. The comprehensive studies described below would not have been possible without this speedup.

A paper describing the modifications in the algorithm is currently in preparation (Pastewka and Robbins 2012a) and an excerpt is included in Appendix I. We will make the implementation available as an open source add-on to LAMMPS. The group maintaining the files developed by Kong et al. (2009) has agreed to update the files to include our improvements and we are also talking to the developers of LAMMPS (lammmps.sandia.gov) about incorporating it in future releases.

2. MOLECULAR DYNAMICS SIMULATIONS OF SINGLE ASPERITY CONTACT

One thrust has been molecular dynamics (MD) studies of contacts between a single spherical asperity and a substrate, or between two flat surfaces. In addition to providing understanding of the nature of these contacts at the atomic scale, these simulations provide tests of continuum models of contact that can be used to study multi-asperity contacts on larger length scales.

Three specific studies are described below. The first examines the profound affect that a single layer of adsorbed atoms can have on contact and friction. The second shows that thermal fluctuations lead to large pressures that suppress the number of contacting atoms by orders of magnitude. Finally the effect of contact and tip size on the friction coefficient is evaluated.

Adsorbed Monolayers

One study (Cheng et al. 2010) examined the effect of adsorbed monolayers on a spherical tip with a radius R that is typical of atomic force microscope (AFM) experiments. Previous studies of bare surfaces showed that the atomic scale deviations from a sphere that are present on any tip constructed from discrete atoms lead to significant deviations from continuum theory and dramatic variability in friction forces (Luan and Robbins 2005, 2006). However surfaces are rarely bare. Most are coated by a monolayer of water, hydrocarbon or other adsorbed material after any exposure to air.

We found that introducing an adsorbed monolayer leads to larger deviations from continuum theory, but decreases the variations between tips with different atomic structure. Although the film is fluid, it remains in the contact and behaves qualitatively like a thin elastic coating except for certain tips at high loads. Some specific findings that are detailed in the paper are:

- 1) The contact area increases dramatically with a single molecular layer (Fig. 1). The area at the lowest load studied was higher than the highest area predicted by continuum theory.
- 2) The contact stiffness is reduced by an order of magnitude for small displacements, but approaches the continuum result at large displacements. The extra compliance comes from compression of the monolayer but is equivalent to continuum results for a thicker layer that is much softer than the solid.
- 3) Monolayers naturally lead to a friction that scales linearly with load, much as was seen for flat surfaces (He et al. 1999, Muser et al. 2001). In contrast, bare surfaces exhibit very different scaling with load and friction forces that vary by two orders of magnitude (Luan and Robbins 2005, 2006).

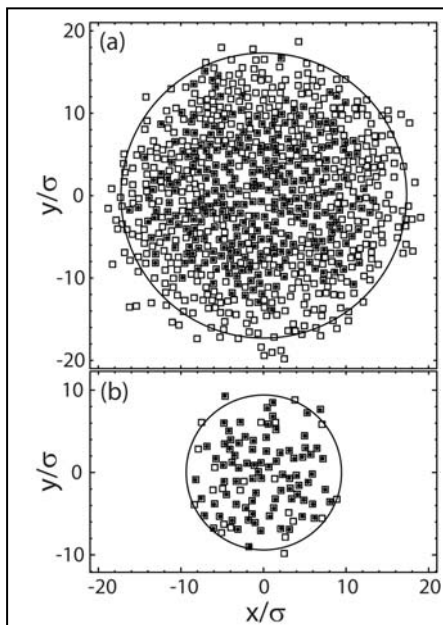


Figure 1. Squares show contacting atoms (a) with an adsorbed monolayer and (b) without a monolayer. The load and all other parameters are the same and $\sigma \sim 0.3\text{nm}$ is an atomic diameter.

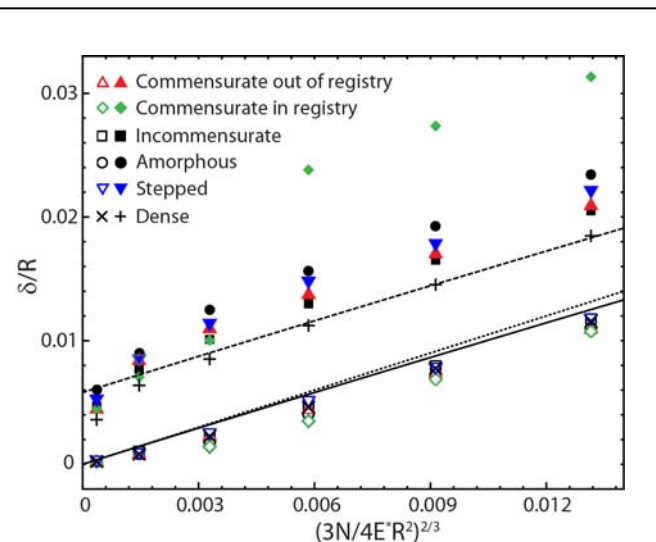


Figure 2. Displacement δ of tip (closed symbols) and substrate (open symbols) for different tip geometries and continuum prediction (solid line). The much larger tip displacement indicates a low stiffness from compression of the adsorbed layer. R is the tip radius, N the load and E^* the effective contact modulus.

Effect of Thermal Fluctuations on Contact

Thermal fluctuations are generally ignored in continuum treatments of contact mechanics and in many simulations that attempt to test continuum theories at atomic scales. A detailed study (Cheng and Robbins 2010b) of the effect of thermal fluctuations on contact was completed for the simplest possible geometry – two atomically flat surfaces. The results show that it is very difficult to extend the continuum definition of contact area to atomic scales. The results were then shown to describe single asperity contact of a sphere on a plane.

The flat surfaces were (001) surfaces of fcc crystals with the same (commensurate) or different (incommensurate) lattice constants. An amorphous surface obtained by removing all atoms above a reference plane was also considered. From a continuum perspective the true area of contact between such atomically-flat, nonadhesive, surfaces should be equal to the apparent area at any positive load. However, simulations show that the fraction of atoms experiencing a contact force at any instant in time is orders of magnitude smaller than unity and rises roughly linearly with load over several decades in load.

Fig. 3 illustrates results for the three types of surfaces. The x-axis corresponds to the compressive strain perpendicular to the surface and extends up through the range associated with the hardness of typical materials. Yield usually occurs at strains of 10^{-4} to 10^{-2} and the fraction of area in contact rises linearly from about 0.3% to 30% over this range. Even the fraction of atoms that contact at any instant of the entire simulation (triangles) remains well below unity except in the very special case of two identical flat crystals (Fig. 3a).

These counterintuitive results are quantitatively explained by a very simple model for thermal vibrations (solid lines in Fig. 3 and 4). Each atom feels a potential well from its surface that can be approximated by a single spring k_{eff} . From dimensional analysis, this must be $k_{\text{eff}} = cA_a E^* / \sigma$ where σ is the molecular diameter, A_a the surface area per atom, E^* the contact modulus and c a constant of order unity. The simulations showed $c=0.92$ for Lennard-Jones interactions. The thermal pressure associated with the rms thermal fluctuation x_{rms} about the lattice site is:

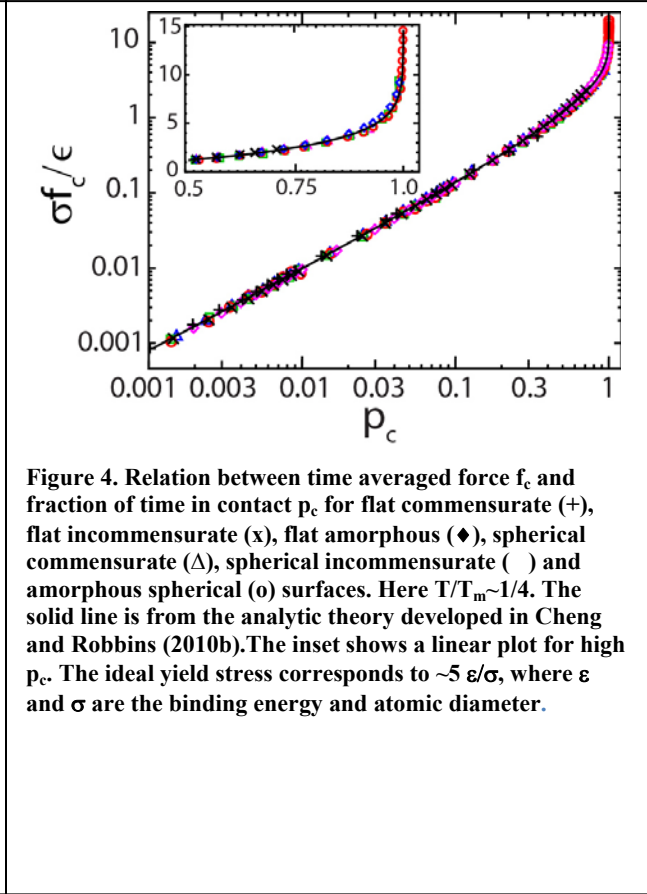
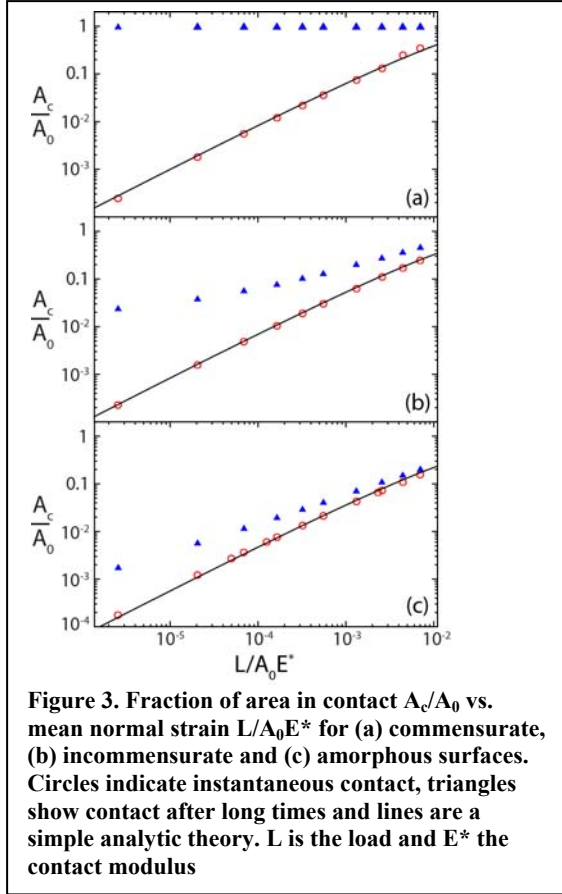
$$p_T = k_{\text{eff}} x_{\text{rms}} / A_a = cE^* (x_{\text{rms}} / \sigma).$$

From the Lindemann criterion, x_{rms} / σ is 10% at the melting temperature T_m , and rises as $T^{0.5}$. Thus $p_T / E^* \approx 0.1 (T/T_m)^{0.5}$ and the fraction of area required to support a normal load L is

$$\frac{A_c}{A_0} \approx 10 \sqrt{T_m / T} \frac{L}{A_0 E^*} \quad (1)$$

This simple argument is in reasonable agreement with Fig. 3 where $T/T_m \approx 1/4$.

The analytic argument produces two other predictions that are confirmed by the simulations. One is that the distribution of local forces at any instant has a simple exponential form. The second is that the time averaged force on an atom f_c is directly related to the fraction of time p_c that it is in contact. As illustrated in Fig. 4, this relation is independent of whether the atom is on a commensurate, incommensurate or amorphous surface and whether the surface is flat or spherical. Note that the force must be close to the ideal yield stress before atoms spend more than half their time in contact and the actual yield stress is typically orders of magnitude smaller.



Scale Dependence of Friction

Traditional continuum theories of single asperity contact have no intrinsic microscopic length scale. All results depend only on ratios of macroscopic lengths such as the radius of curvature R and contact radius a (Johnson 1985). Hurtado and Kim (1999a, 1999b) suggested that friction should be scale dependent in certain limits. They argued that contacts could advance through propagation of dislocations across the interface rather than uniform sliding. The Burgers vector of the dislocation ($\sim \sigma$) and core size of the dislocation introduce microscopic length scales. Just as dislocations reduce the yield stress in bulk crystals, dislocations led to a reduced, scale dependent friction.

In addition to lowering friction, Hurtado and Kim's model provided a scale dependent mechanism for partial slip, where sliding occurs within the outer ring of a contact and gradually spreads inwards. The previous Cattaneo-Mindlin theory for partial slip does not have a microscopic length scale (Johnson 1985). Improved understanding of partial slip was a motivation of the proposed research, because it is a major source of damping in mechanical joints, including mounts for aircraft engines (Segalman 2006).

Testing the scale dependence proposed by Hurtado and Kim poses significant challenges. They predicted that the friction would drop roughly as $(a/\sigma)^{-1/2}$ over scales from $a/\sigma \sim 10^2$ to 10^4 . Since R must be bigger than $10a$ to be in the linear elastic limit, this means linear dimensions of 10^3 to $10^5 \sigma$ are required. Gao (2010) extended Hurtado and Kim's work and found transitions at length scales about an order of magnitude smaller, but still taxing for standard atomistic simulations.

Using the Green's function method described above, Ligneres and Robbins (2012) examined the friction between spherical tips of radius R/σ between 50 and 6000 ($\sim 2\mu\text{m}$). The results are very different than envisioned by any of the previous continuum theories and are currently being prepared for publication. The main findings are:

- 1) The mechanism of sliding is never dislocation or partial slip as envisioned by the Cattaneo-Mindlin, Hurtado-Kim and Gao models. The Peierls barrier for advance of the dislocation is too small to pin dislocations that are formed in response to shear stress.
- 2) The area and load dependence of friction forces depends on the precise geometry of the tips.
- 3) For incommensurate tip/substrate pairs (different lattice constants), the friction is small, nonuniversal and rises less than linearly with area and load.
- 4) The commensurate case of equal lattice constants is the only one that allows for the surface dislocations in Hurtado and Kim's treatment. Once the static friction is exceeded the entire tip advances by a distance of order σ because dislocations cannot be pinned.
- 5) The friction coefficient is not only a function of a/σ , as in the results of Hurtado and Kim and of Gao. There is an explicit dependence on R that is completely absent in their models.
- 6) Fig. 5 shows that the static friction coefficients for commensurate systems of all sizes collapse onto a universal curve as a function of $a/(R\sigma)^{1/2}$. Detailed analysis shows that the local slope of the surface (a/R) plays a role in the force at which the tip can advance.

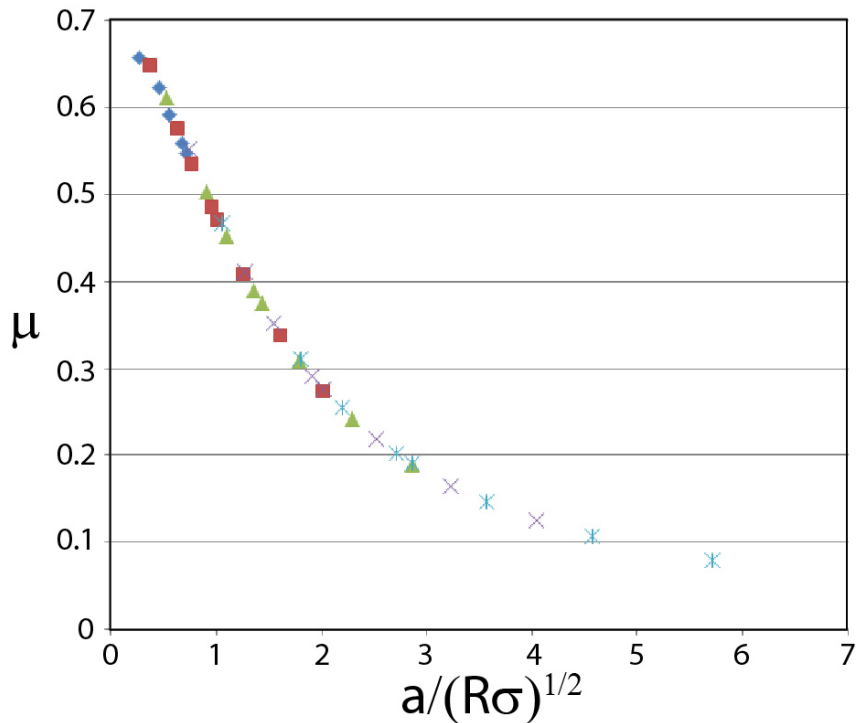


Figure 5. Friction coefficient μ as a function of $(a^2/R\sigma)^{1/2}$ for tips with radius R/σ equal to 300 (\blacklozenge), 600 (\blacksquare), 1200 (\blacktriangle), 2400 (\times) and 4800 ($*$). The coefficient of friction is just less than 0.7 for flat surfaces with the same spacing and interactions.

MULTIASPERITY CONTACT

Macroscopic surfaces are typically rough on a wide range of scales, often from less than a micrometer to more than a millimeter. The presence of roughness on a wide range of length scales has profound effects on contact and friction between experimental surfaces. Under a broad range of conditions, the area of intimate contact between nonadhesive rough surfaces A_c is orders of magnitude smaller than the apparent surface area A_0 and rises linearly with applied load L . This proportionality between area and load, and an assumption of a constant yield stress in contacts, provides the most common explanation (Johnson, 1985) for Amontons' laws that friction is proportional to load and independent of A_0 . Because A_c is small, the interfacial region is very compliant. In applications from jet engine mounts to micro-electromechanical systems (MEMS), the interfacial compliance can significantly reduce the stiffness of joints formed by pressing two components together (Segalman et al. 2006). Electrical and thermal conductances are also strongly affected.

Dimensional analysis implies that the linear relation between area and load has the form:

$$A_c = \kappa L / E^* h'_{\text{rms}} \quad (2)$$

where κ is a constant of order unity, the contact modulus E^* characterizes the elastic response of the substrate, and the rms surface slope h'_{rms} is a dimensionless quantity characterizing roughness. Numerical tests show κ has a constant value of about 2 for most surfaces (Hyun et al. 2004). One of the goals of the grant was to develop equations like Eq. (2) that describe the stiffness of contacts and test them with numerical calculations. A second was to include the effect of adhesion on contact area.

The following sections describe the three major studies undertaken during the grant. The first calculated the spatial correlations between contacting regions in order to test analytic theories of contact area. The results show that conventional models give qualitatively wrong correlations because they neglect asperity interactions. The second develops and tests a very simple model that describes the stiffness of mechanical contacts between rough, nonadhesive surfaces. The final study has resulted in a very simple and robust picture for the contact area between rough, adhesive surfaces. The model explains why adhesion between most macroscopic surfaces is so weak, and provides a simple dimensionless number that predicts when adhesion will be strong.

Statistics of Asperity Heights

A wide variety of natural and man-made surfaces exhibit self-affine fractal roughness. Examples include common machined surfaces, fracture surfaces and surfaces formed by deposition or erosion (Mandelbrot 1982, Greenwood 1984, Meakin 1998). The hallmark of self-affine surfaces is that the change in height h over a lateral length l scales as a power law: $h \propto l^H$, where H is called the Hurst exponent. For typical experimental surfaces, H ranges from 0.5 to 0.8. A random walk gives $H=0.5$.

Calculations for the contact geometry have traditionally been based on the bearing area model (Johnson 1985). The problem of contact between two rough surfaces can be mapped to contact between a rough and flat surface (Johnson 1985). At a given separation h_0 between surfaces, contact is assumed to occur wherever the rough surface would interpenetrate the flat surface. This corresponds to the set of points above h_0 on the rough surface. The widely used Greenwood-Williamson (1966) model and generalizations, calculate the load required to bring this region into contact without including the affects of elastic interactions between asperity peaks.

Persson (2001,2007) has recently developed a scaling theory for contact that includes asperity interactions in an approximate manner. These interactions can be important because the deformation produced by a force on an asperity decays only as the inverse separation. This means that nearby areas are unlikely to make the next contact.

Despite the large difference between the Greenwood-Williamson and Persson models they give similar results for the total contact area. The respective values of κ are about 2.5 and 1.6 compared to the numerical result of 2 (Hyun et al. 2004). This similarity in total area makes it interesting to compare the spatial correlations in the contacting regions in order to distinguish between the two models.

In recent papers (Hyun and Robbins 2007, Campana et al. 2008) we studied the square of the Fourier transform of the contacting region, which gives the Fourier transform of the contact-contact correlation function $S(q)$. Results from elastic calculations that include asperity interactions yield $S(q) \propto q^{-(1+H)}$ for a wide range of H . Persson later showed that his calculation gave the same scaling exponent (Persson 2008).

During the grant we calculated the correlation function $S(q)$ for the bearing area model using numerical results and an analytic theory (Ramiseti et al. 2011). Both gave $S(q) \propto q^{-(2+H)}$ rather than the correct result for interacting asperities $S(q) \propto q^{-(1+H)}$. This failure of the bearing area model has important physical consequences. For example, almost all area in the bearing area model is in the largest connected regions, while most area is in the smallest connected regions of the full elastic calculation. This leads to very different results for measurable quantities such as contact conductance of heat and electricity, as well as very different predictions for adhesion.

Mechanical Stiffness of Multiasperity Contacts

The component of the stiffness coming from the interface between rough solids was calculated for surfaces with a wide range of Hurst exponents using fully atomistic calculations and the Green's function method. A simple relation like Eq. (2) described all the results quite accurately (Akarapu et al. 2011) and can be used to predict the response of experimental surfaces.

The interfacial stiffness k is found to scale linearly with the applied load L . Since k is the opposite of the derivative of load with separation u , one must have a relation like:

$$k = -dL/du = L/\gamma h_{\text{rms}} \quad (3)$$

where γ is a constant of order unity and the rms height h_{rms} is a natural length scale characterizing the surface. This type of relation had been suggested by Berthoud and Baumberger (1997) and Persson (2007). Our simulations provide the first detailed numerical test of Eq. (3). As shown in Fig. 6 this relation is quite general, with γ near 0.5. Several other aspects of the results are more surprising:

- 1) The simulations included both perfectly elastic systems treated with Green's functions and atomistic systems that deformed plastically, yet the two cases gave similar values of κ and γ . A detailed analysis indicates that plasticity is confined to regions near the surface. It is important in eliminating extremely large local pressures but does not affect the long-range scaling (Sharp et al. 2012).
- 2) Atomic steps affect plasticity but have much less influence on the total area than in two dimensional studies (Luan 2009).
- 3) The lateral stiffness k_T associated with elastic deformation of the contacts can be larger than the normal stiffness k_N . Continuum theory predicts the opposite, but does not include lattice anisotropy.

- 4) The stiffness only depends on the lateral position of contacting regions and not on the height variations or other factors. This was used to derive a linear relation between area and a normalized stiffness k^* (Fig. 7).
- 5) There is an additional compliance associated with relative motion of contacting atoms at the interface. This atomistic compliance has almost no affect on the normal stiffness (Fig. 7a), but can reduce the lateral stiffness and friction by orders of magnitude (Fig. 7b). The results are analogous to single asperity results of Luan and Robbins (2005,2006). A scaling study indicates that atomistic effects can be an important factor in macroscopic samples (Akarapu et al. 2011).

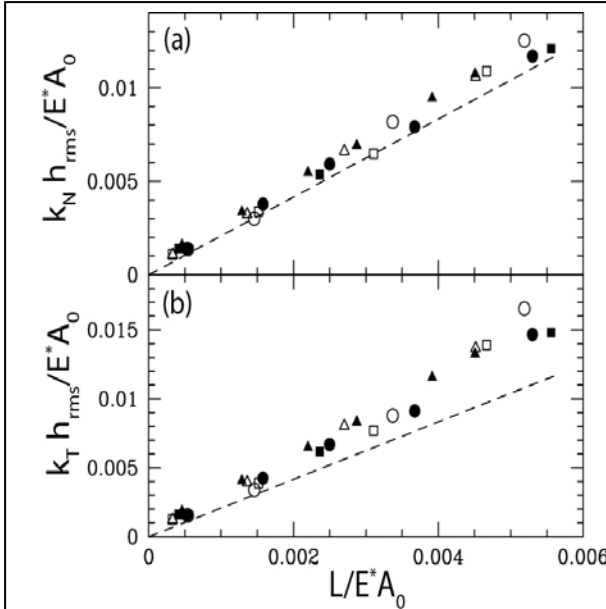


Figure 6. The scaled (a) normal stiffness and (b) transverse stiffness as a function of scaled load. Results are for $H=0.5$ (open symbols) and $H=0.8$ (filled symbols) in systems with linear dimension of 189.2σ (\circ), 94.6σ (\square), or 47.3σ (Δ). Dashed lines have slope $1/\gamma$ with $\gamma=0.48$.

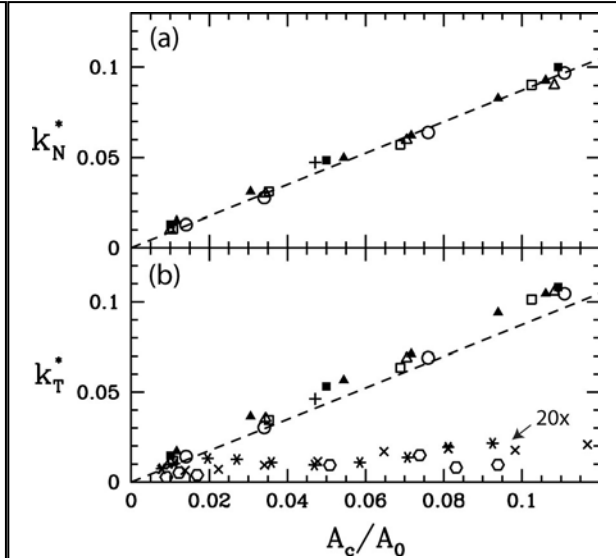


Figure 7. The scaled (a) normal stiffness and (b) transverse stiffness as a function of A_c/A_0 . Results are for $H=0.5$ (open symbols) and $H=0.8$ (filled symbols) in systems with linear dimension of 189.2σ (\circ), 94.6σ (\square), or 47.3σ (Δ). Pluses show Green's function results. The total transverse stiffness, multiplied by 20 to make it visible, is shown for 189.2σ systems with $H=0.5$ (\times) or 0.8 (hexagons) and a triangular lattice with $H=0.8$ ($*$). Dashed lines have slope 0.87.

Adhesive Contact Between Rough Surfaces

Adhesive van der Waals interactions are present between almost all surfaces. The forces required to break these interactions are in the MPa range, and enable Geckos to climb walls (Autumn 2006) and tape or putty to stick to surfaces. Similar forces are present between nearly all surfaces around us, and yet we rarely observe adhesive forces when we lift objects off of tables. Fuller and Tabor resolved this adhesion paradox by showing that surface roughness prevents adhesion by limiting the area that can come into contact (Fuller and Tabor 1975). However a detailed theory for this suppression and a criterion for the presence of adhesion for soft materials has remained lacking.

We have used the Green's function technique described above to explore a full range of parameter space with different rms roughness h_0 , rms slope h'_0 , Hurst exponent H , adhesion energy γ , adhesion range Δ_c and system size. The results guided the development of a simple

scaling theory that captures all our simulations and provides a simple prediction for when adhesion will occur and how the contact area scales with load. The work is being prepared for publication (Pastewka and Robbins, 2012b) and a draft is provided in Appendix II.

One important finding is that the portion of the surface that experiences repulsive forces, A_{rep} , is always fractal and has a characteristic width w that is comparable to the smallest scale of surface roughness. As a result, the perimeter of the repulsive region $P=\beta A_{rep}/w$, where β is about 2.8 for all surfaces studied. We also find that the ratio of the A_{rep} to the repulsive load on the same region is given by the same κ as for nonadhesive surfaces.

Given the repulsive area, continuum theory for nonadhesive surfaces (Johnson 1985) can be used to estimate the range R away from the perimeter where attractive forces will be felt. The ratio of repulsive to attractive area $A_{att}=PR$ should then be given by:

$$\frac{A_{rep}}{A_{att}} = \frac{2}{\beta} \left(\frac{h'_0 w}{2\Delta_c} \right)^{2/3} \quad (4)$$

Figure 8 shows that results for all surfaces fall very close to this prediction with $\beta=2.8$.

The total attractive contribution to the load is $N_{att}=A_{att} \gamma/\Delta_c$, since γ/Δ_c is the average adhesive force over the range of interaction. One can define a renormalized κ' that relates the repulsive area to the total load $N=N_{rep}-N_{att}$

$$A_{rep} = \kappa' \frac{N}{h'_0 E^*}$$

Then plugging in the relations above one finds

$$\frac{1}{\kappa'} = \frac{1}{\kappa} + \frac{1}{\kappa_{att}} = \frac{1}{\kappa} - \frac{\beta}{2h'_0} \frac{\delta}{\Delta_c} \left(\frac{2\Delta_c}{h'_0 w} \right)^{2/3} \quad (5)$$

where $\delta = \gamma/E^*$ is a length characterizing the relative strength of adhesion and elasticity. Fig. 9 shows a test of the predictions of this simple relation for a wide range of surfaces.

Equation 5 allows the attractive area to be predicted in terms of a few simple quantities. Adhesion will have negligible effect when the term on the far right is much smaller than $1/\kappa \sim 0.5$. When the right hand side becomes negative, there will be substantial adhesion. Simulations in this limit show a finite repulsive area at zero load, and a negative load is needed to separate the surfaces.

For most solids γ and E^* are determined by the same interactions and $\gamma/E^* < 0.01\sigma$. The range of interactions is typically $\sim 0.1 \sigma$ or larger and the width $w > \sigma$. As a result, the correction from adhesion is negligible unless the rms slope is extremely small. This type of situation may arise in wafer bonding of silica with sub nanometer roughness, but not for most of the surfaces around us.

Tape, putty and elastomeric materials typically have anomalously small moduli because they contain chain molecules that are relatively fluid in between a dilute set of chemical crosslinks. The modulus reflects the entropic cost of stretching chains between crosslinks while γ is determined by van der Waals interactions. As a result, γ/E^* can be four orders of magnitude larger than for other materials and Eq. 4 becomes negative even for typical rough surfaces.

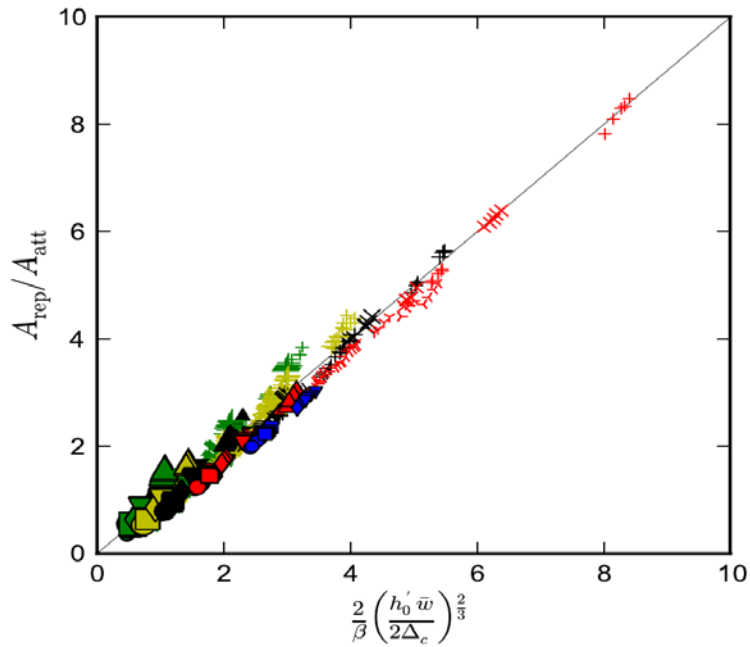


Figure 8. Test of Equation 4 for a wide range of system parameters.

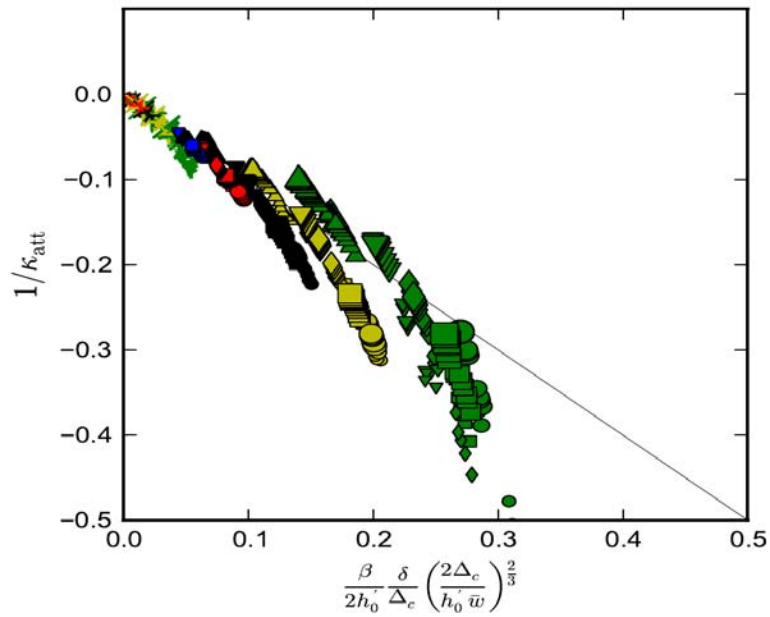


Figure 9. Test of Equation 5 for the same set of systems. Note that as k_{att} approaches -0.5 , and k' approaches zero there is a systematic deviation towards greater adhesion.

PAPERS PUBLISHED

1. S. Cheng, B. Luan and M. O. Robbins, "Contact and Friction of Nano-Asperities: Effects of Adsorbed Monolayers," Phys. Rev. E 81, 016102 (2010). ([10.1103/PhysRevE.81.016102](https://doi.org/10.1103/PhysRevE.81.016102)).
2. S. Cheng and M. O. Robbins, "Defining Contact at the Atomic Scale," Tribol. Lett. **39**, 329-348 (2010). ([Doi:10.1007/s11249-010-9682-5](https://doi.org/10.1007/s11249-010-9682-5)).
3. S. Akarapu, T. Sharp and M. O. Robbins, "Stiffness of Contacts between Rough Surfaces," Phys. Rev. Lett. 106, 204301 (2011). ([10.1103/PhysRevLett.106.204301](https://doi.org/10.1103/PhysRevLett.106.204301)).
4. S. B. Ramisetti, C. Campañá, G. Anciaux, J.-F. Molinari, M. H. Müser and M. O. Robbins, "The autocorrelation function for island areas on self-affine surfaces," J. Phys.: Condens. Matter **23**, 215004 (2011) ([10.1088/0953-8984/23/215004](https://doi.org/10.1088/0953-8984/23/215004)).

PAPERS IN PREPARATION

5. V. Ligneres and M. O. Robbins, 2012. Scale dependence of friction in single-asperity contacts, in preparation.
6. L. Pastewka and M. O. Robbins, 2012a. Multilayer Lattice Green's Functions for Molecular Dynamics, in preparation and Appendix I.
7. L. Pastewka and M. O. Robbins, 2012b. Contact and Adhesion Between Rough Surfaces, in preparation and Appendix II.
8. T. Sharp, L. Pastewka and M. O. Robbins, 2012. Effect of plasticity and atomic steps on rough surface contact, in preparation.

THESES

S. Cheng, "Contact and capillary forces at the atomic scale," Ph. D. Johns Hopkins University, July 9, 2010. (Sections related to AFOSR funded projects are available in the publications listed above.)

Invited Talks on Work Supported by Grant: 3/1/09 – 11/30/2011

- 1) "Friction in Multi-Asperity Contacts and 'Earthquakes' in Sheared Solids," International School on Complexity "Grains, Friction, and Faults," Erice, Sicily, Italy, July 20-25, 2009.
- 2) "Using Simulations to Probe the Atomic Origins of Macroscopic Friction," Plenary Talk, World Tribology Congress 2009, Kyoto, Japan, September 6-11, 2009.
- 3) "Precursor Events and the Onset of Frictional Sliding," Invited Talk, World Tribology Congress 2009, Kyoto, Japan, September 6-11, 2009.
- 4) "Energy Dissipation and the Atomic Origins of Kinetic Friction," Focus Workshop on "Energy Dissipation in Nanocontacts and Molecular Bonds," Dresden, Germany, September 28 - October 1, 2009.
- 6) "Friction: A Surprisingly Slippery Subject," Colloquium, Duke University, Nov. 11, 2009.
- 7) "Friction: A Surprisingly Slippery Subject," Colloquium, Brandeis University, January 19, 2010.
- 8) "Connecting atomistic and continuum models of contact area and stick-slip friction in single and multi-asperity contacts," CECAM Workshop: Stick-slip dynamics, from nano to geophysical scales, Lausanne, Switzerland, May 3-5, 2010.
- 9) "Contact and Friction of Nano-Asperities," STLE Annual Meeting, Las Vegas, May 16-20, 2010.

- 10) "Coupling Atomistic and Continuum Descriptions in Multi-scale Modeling," UCSB-IMMS Workshop on Multiscale Modeling and Coarse-Graining, Santa Barbara, CA, June 4, 2010
- 11) "Connecting Atomistic and Continuum Models of Contact Area, Stiffness and Friction in Single and Multi-Asperity Contacts," MMM2010, Freiburg, Germany, October 7-10, 2010
- 12) "Friction: A Surprisingly Slippery Subject," Highlight Seminar, Thomas Young Centre, Imperial College London, Dec. 9, 2010
- 13) "Friction forces from atomic to macroscopic scales," XXXIV Encontro Nacional de Fisica da Materia Condensada, Iguassu Falls, Brazil, June 5-10, 2011.
- 14) "Exploring the Atomic Underpinnings of Macroscopic Friction," Keynote Lecture at Joint ICTP-FANAS Conference on Trends in Nanotribology, Trieste, Italy, Sept. 12 - 16, 2011.
- 15) "Contact, Adhesion and Friction Between Self-Affine Surfaces: Does Friction Scale with Contact Area?" Statistical Physics Seminar, University of Maryland, Oct. 18, 2011.
- 16) "Scaling of Area, Stiffness and Friction for Multi-Asperity Contacts," Keynote Lecture, International Tribology Conference, Hiroshima, Japan, Oct. 30 - Nov. 3, 2011.

Contributed Talks and Posters:

- 1) "Measuring Contact Area at the Nanometer Scale," S. Cheng and M. O. Robbins, Focus Session: Tribophysics – Sliding Friction, March Meeting of the American Physical Society, March 15-19, 2010, Portland OR.
- 2) "Non-Adhesive Elastic Contact Between a Rigid Self-affine Fractal Surface and an Elastic Manifold: 3D Atomistic Simulation," S. Akarapu and M. O. Robbins, Gordon Conference on Tribology, Waterville, ME, June 27-July1, 2010.
- 3) "Defining Contact at Atomic Scales," S. Cheng and M. O. Robbins, Gordon Conference on Tribology, Waterville, ME, June 27-July1, 2010.
- 4) "Molecular Dynamics Simulations of Single Asperity Contact," V. Ligneres, Gordon Conference on Tribology, Waterville, ME, June 27-July1, 2010.
- 5) "Stiffness of Contacts of Self-Affine Surfaces," T. A. Sharp, M. O. Robbins and S. Akarapu, Focus Session: Friction, Fracture and Deformation Across Length Scales, March Meeting of the American Physical Society, March 21-25, 2011, Dallas, TX.
- 6) "Onset of Sliding in Single Asperity Contacts," V. Ligneres and M. O. Robbins, Focus Session: Friction, Fracture and Deformation Across Length Scales, March Meeting of the American Physical Society, March 21-25, 2011, Dallas, TX.
- 7) "Contact of Adhesive, Randomly Rough Surfaces," L. Pastewka and M. O. Robbins, Materials Research Society Fall Meeting, Nov. 28, 2011.
- 8) "Effect of Atomic Scale Geometry on Contact and Friction Between Rough Solids," T. Sharp, M. O. Robbins and L. Pastewka, March Meeting of the American Physical Society, February 27-March 2, 2012, Boston, MA.
- 9) "Adhesive Contact of Randomly Rough Surfaces," L. Pastewka and M. O. Robbins, March Meeting of the American Physical Society, February 27-March 2, 2012, Boston, MA.

REFERENCES

- S. Akarapu, T. Sharp and M. O. Robbins, 2011. "Stiffness of Contacts between Rough Surfaces," *Phys. Rev. Lett.* 106, 204301.
- K. Autumn, 2006. How Gecko Toes Stick, *American Scientist* 94, 124-132.
- P. Berthoud and T. Baumberger, 1997. Shear stiffness of a solid-solid multicontact interface, *Proc. R. Soc. Lond. A* 454, 1616-1634.
- C. Campana and M. H. Muser, 2006. Practical Green's Function Approach to the Simulation of Elastic, Semi-Infinite Solids, *Phys. Rev. B* 74, 075420.
- C. Campaña, M. H. Muser, and M. O. Robbins, 2008. Elastic contact between self-affine surfaces: Comparison of numerical stress and contact correlation functions with analytic predictions, *J. Phys.: Condens. Matter* **20**, 354013.
- S. Cheng, B. Luan and M. O. Robbins, 2010. Contact and Friction of Nano-Asperities: Effects of Adsorbed Monolayers," *Phys. Rev. E* 81, 016102.
- S. Cheng and M. O. Robbins, 2010. Defining Contact at the Atomic Scale, *Tribology Letters* **39**, 329-348.
- K. N. G. Fuller and D. Tabor, 1975. The Effect of Surface Roughness on the Adhesion of Elastic Solids, *Proc. R. Soc. Lond. A* 345, 327.
- Y. Gao, 2010. A Peierls perspective on mechanisms of atomic friction, *J. Mech. Phys. Solids* 58, 2023-2032.
- J. A. Greenwood and J. B. P. Williamson, 1966. Contact of nominally flat surfaces, *Proc. R. Soc. London, Ser. A* 295, 300-319.
- J. A. Greenwood, 1984. A unified theory of surface roughness, *Proc. R. Soc. Lond. A* 393, 133-157.
- G. He, M. H. Muser and M. O. Robbins, 1999. Adsorbed Layers and the Origin of Static Friction, *Science* **284**, 1650-1652.
- J. A. Hurtado and K.-S. Kim, 1999a. Scale effects in friction of single-asperity contacts. I. From concurrent slip to single-dislocation-assisted slip. *Proc. R. Soc. London A* 455, 3363- 3384.
- J. A. Hurtado, K.-S. Kim, 1999b. Scale effects in friction of single-asperity contacts. II. Multiple-dislocation-cooperated slip. *Proc. R. Soc. London A* 455, 3385-3400.
- S. Hyun, L. Pei, J.-F. Molinari and M. O. Robbins, 2004. Finite-element analysis of contact between elastic self-affine surfaces, *Phys. Rev. E* 70, 026117.

- S. Hyun and M. O. Robbins, 2007. Elastic Contact Between Rough Surfaces: Effect of Roughness at Large and Small Wavelengths, *Tribology International*, **40**, 1413-1422.
- K. L. Johnson, 1985. *Contact Mechanics* (Cambridge, New York)
- L. T. Kong, G. Bartels, C. Campana, C. Denniston and M. H. Muser, 2009. Implementation of Green's function molecular dynamics: An extension to LAMMPS, *Computer Physics Communications* 180 (6), 1004-1010.
- V. Ligneres and M. O. Robbins, 2012. Scale dependence of friction in single-asperity contacts, in preparation.
- B. Luan and M. O. Robbins, 2005. The breakdown of continuum models for mechanical contacts, *Nature* **435**, 929-932.
- B. Luan and M. O. Robbins, 2006. Contact of Single Asperities with Varying Adhesion: Comparing Continuum Mechanics to Atomistic Simulations, *Phys. Rev. E* **74**, 026111.
- B. Luan and M. O. Robbins, "Hybrid Atomistic/Continuum Study of Contact and Friction Between Rough Solids," *Tribol. Lett.*, **36**, 1-16 (2009).
- B. B. Mandelbrot, 1982. *The Fractal Geometry of Nature*. (Freeman, New York).
- P. Meakin, 1998. *Fractals, scaling and growth far from equilibrium*. (Cambridge, 1998).
- M. H. Müser, L. Wenning, and M. O. Robbins, 2001. Simple Microscopic Theory of Amontons' Laws for Static Friction, *Phys. Rev. Lett.* 86, 1295-1298.
- L. Pastewka and M. O. Robbins, 2012a. Multilayer Lattice Green's Functions for Molecular Dynamics, in preparation.
- L. Pastewka and M. O. Robbins, 2012b. Contact and Adhesion Between Rough Surfaces, in preparation.
- B. N. J. Persson, 2001. Theory of rubber friction and contact mechanics, *J. Chem. Phys.* 115: 3840.
- B. N. J. Persson, 2008. On the elastic energy and stress correlation in the contact between solids with randomly rough surfaces, *J. Phys.: Condens. Matter*, 20:312001.
- B. N. J. Persson, 2007. Relation between Interfacial Separation and Load: A General Theory of Contact Mechanics, *Phys. Rev. Lett.* 99, 125502.
- S. B. Ramisetty, C. Campaña, G. Anciaux, J.-F. Molinari, M. H. Müser and M. O. Robbins, 2011. The autocorrelation function for island areas on self-affine surfaces, *J. Phys.: Condens. Matter* **23**, 215004.

D. J. Segalman, L. A. Bergman, D. J. Ewins, 2006. Report on the SNL/NSF International Workshop on Joint Mechanics, Arlington, Virginia, 16-18 October 2006. Sandia Report: SAND2007-7761.

APPENDICES

I. METHODOLOGY FOR CONTACT MECHANICS OF CRYSTAL LATTICES

Analysis of the response of an isotropic elastic half-space to spherical contact geometries and point forces goes back to the work of Hertz [1], Boussineq and Cerruti in the 19th century. Since then, continuum expressions have been derived for various contact geometries [2], and have become indispensable tools in mechanical engineering. Continuum mechanical contact theories, however, break down at the atomic scale [3]. Yet, an understanding of long-ranged elastic deformations of the bulk down to the atomic scale is important, for example, for the interpretation of scanning probe experiments or the contact stiffness of atomically rough surfaces [4]. Also, chemi- and physisorption processes at crystal surfaces can be appreciably influenced by the elastic response of the supporting solid.

Here, we develop a transfer matrix formulation of the Green's function that can be used to renormalize the elastic interaction of any crystalline solid for which the dynamical matrix is known. Such transfer matrix formulations have been traditionally used in the analysis of the electronic [5] and phononic [6] structure of surfaces, but have to the best of our knowledge not been discussed in the context of interactions that reach farther than nearest neighbors. Such long-ranged interactions are necessary for a realistic description of materials. Hence, the treatment of long-ranged interactions allows to employ the renormalized half space as an ideally matched elastic boundary in atomistic calculations.

A. Elastic surface Green's functions

1. Green's function of the full dynamical system

Let us expand vibrations of the crystalline solid around the ground-state configuration $\vec{r}_{i\alpha}^0$ of each atom $i\alpha$. To obtain the usual harmonic approximation, we write all dynamical equations in terms of the displacement $\vec{u}_{i\alpha}$ of atom $i\alpha$ from its ground-state position. Here and in the following, atoms are indexed by $i\alpha$ where α is a layer index (as counted from the surface of the crystal where $\alpha = 0$) and i denotes inequivalent atoms within each layer. The full dynamical Green's function can then be obtained from the Fourier transform of the dynamical equation

$$m \frac{\partial^2 \vec{u}_{i\alpha}}{\partial t^2} + \sum_{j\beta} \mathbf{D}_{i\alpha j\beta} \vec{u}_{j\beta} = f_{i\alpha}. \quad (1)$$

APPENDICES

Here, m is the mass of each atom and we limit ourselves to the treatment of a single atomic species. A generalization of the following procedure to multi-species unit cells is straightforward.

We now treat the dynamical equation in reciprocal space parallel to the surface and in real space perpendicular. With

$$\vec{u}_{i\alpha}(t) = \int \frac{d^3q}{(2\pi)^3} \frac{d\omega}{2\pi} \vec{u}(\vec{q}) e^{i\vec{q}\cdot\vec{r}_{i\alpha} + i\omega t}, \quad (2)$$

where \vec{q} lies in the plane of the surface and $\vec{r}_{i\alpha} = \vec{r}_{i\alpha}^0 + \vec{u}_{i\alpha}$ is the position of atom $i\alpha$, we find

$$\vec{F}_{i\alpha} = \sum_{\beta} \int \frac{d^3q}{(2\pi)^3} \frac{d\omega}{2\pi} e^{i\omega t} \vec{u}_{\beta}(\vec{q}, \omega) \sum_{j\beta} \mathbf{D}_{i\alpha j\beta} e^{i\vec{q}\cdot\vec{r}_{j\beta}} \quad (3)$$

$$= \sum_{\beta} \int \frac{d^3q}{(2\pi)^3} \frac{d\omega}{2\pi} e^{i\vec{q}\cdot\vec{r}_{i\alpha} + i\omega t} \vec{u}_{\beta}(\vec{q}, \omega) \sum_{j\beta} \mathbf{D}_{i\alpha j\beta} e^{i\vec{q}\cdot\vec{r}_{j\beta i\alpha}} \quad (4)$$

with $\vec{F}_{i\alpha} = \sum_{j\beta} \mathbf{D}_{i\alpha j\beta} \vec{u}_{j\beta}$ and $\vec{r}_{j\beta i\alpha} = \vec{r}_{j\beta} - \vec{r}_{i\alpha}$. From Eq. (4) we identify

$$\mathbf{D}_{\alpha\beta}(\vec{q}) = \sum_{n\beta \in \text{neighb.}} \mathbf{D}_{i\alpha n\beta} e^{i\vec{q}\cdot\vec{r}_{n\beta i\alpha}} \quad (5)$$

where n run over those neighbors in layer β where $\mathbf{D}_{i\alpha n\beta} \neq 0$ and $\vec{r}_{i\alpha n\beta}$ is the distance vector to those neighbors. In combination with the dynamical Eq. (1) this yields the eigenvalue equation

$$(-m\omega^2 + \mathbf{D}(\vec{q})) \vec{u}(\vec{q}, \omega) = \vec{f}(\vec{q}, \omega) \quad (6)$$

for the permissible modes, and the equation

$$\mathbf{1} + m\omega^2 \mathbf{G}(\vec{q}, \omega) = \mathbf{D}(\vec{q}) \mathbf{G}(\vec{q}, \omega) \quad (7)$$

for the dynamical Green's function $\mathbf{G}(\vec{q}, \omega)$.

In the remainder of this paper we concern ourselves with the static response only. The static response is given by the limit $\omega = 0$, such that the governing equation becomes

$$\mathbf{D}(\vec{q}) \mathbf{G}(\vec{q}) = \mathbf{1}, \quad (8)$$

where we dropped the frequency variable ω for brevity. In order to understand the displacements $\vec{u}_0(\vec{q})$ of the surface layer due to an external force $\vec{f}_0(\vec{q})$ we only need the Green's

APPENDICES

function $\mathbf{G}_{00}(\vec{q})$ element that couples the surface layer to itself. It is usually beneficial to treat the surface stiffness $\Phi(\vec{q}) = \mathbf{G}_{00}^{-1}(\vec{q})$, such that

$$\vec{f}_0(\vec{q}) = \Phi(\vec{q})\vec{u}_0(\vec{q}), \quad (9)$$

instead. Eq. (9) resembles Hooke's law, and the coefficients Φ can be regarded as renormalized spring constants that govern the response of the elastic half space. Note that even though the atomistic interaction within the bulk may be short ranged, real space Φ coefficients typically couple the surface over all length scales.

In the following we assume that the total crystal consists of $N + 1$ identical crystal layers. Then $\mathbf{U}(\vec{q}) = \mathbf{D}_{i\alpha n\alpha}(\vec{q})$, the dynamical matrix that couples within each layer, $\mathbf{V}(\vec{q}) = \mathbf{D}_{i\alpha n(\alpha+1)}$, the matrix coupling to the nearest layers beneath, and $\mathbf{V}^\dagger(\vec{q})$, the matrix coupling to the nearest layer above, do not depend on the index α for $\alpha > 0$. For $\alpha = 0$ we introduce $\mathbf{U}_0(\vec{q}) = \mathbf{D}_{i0n0}$ and note that $\mathbf{V}_0 = \mathbf{V}$. Here \dagger denotes the Hermitian conjugate.

The dynamical matrix then assumes the form

$$\mathbf{D} = \begin{pmatrix} \mathbf{U}_0 & \mathbf{V} & 0 & \cdots & 0 & 0 \\ \mathbf{V}^\dagger & \mathbf{U} & \mathbf{V} & \cdots & 0 & 0 \\ 0 & \mathbf{V}^\dagger & \mathbf{U} & \cdots & 0 & 0 \\ \vdots & \vdots & \vdots & \ddots & \vdots & \vdots \\ 0 & 0 & 0 & \cdots & \mathbf{U} & \mathbf{V} \\ 0 & 0 & 0 & \cdots & \mathbf{V}^\dagger & \mathbf{U}_N \end{pmatrix}, \quad (10)$$

where we dropped the explicit \vec{q} dependence for brevity. For simplicity, we assume no coupling between next-nearest layers, and later show that next-nearest layer interactions can be straightforwardly mapped on a theory that only treats nearest layers. We now give two equivalent formulations that lead to the renormalized surface Green's function.

APPENDICES

2. Displacement transfer matrix formulation

The displacement transfer formulation starts from Eq. (6) with $\omega = 0$. We can write this equation explicitly as

$$\mathbf{U}_0 \vec{u}_0 + \mathbf{V} \vec{u}_1 = \vec{f} \quad (11)$$

$$\mathbf{V}^\dagger \vec{u}_0 + \mathbf{U} \vec{u}_1 + \mathbf{V} \vec{u}_2 = 0$$

$$\mathbf{V}^\dagger \vec{u}_1 + \mathbf{U} \vec{u}_2 + \mathbf{V} \vec{u}_3 = 0$$

$$\vdots$$

$$\mathbf{V}^\dagger \vec{u}_{n-1} + \mathbf{U} \vec{u}_n + \mathbf{V} \vec{u}_{n+1} = 0 \quad (12)$$

$$\vdots$$

$$\mathbf{V}^\dagger \vec{u}_{N-1} + \mathbf{U}_N \vec{u}_N = 0 \quad (13)$$

It is straightforward to see that this set of equations can be expressed as

$$\begin{aligned} \begin{pmatrix} \vec{u}_n \\ \vec{u}_{n-1} \end{pmatrix} &= \begin{pmatrix} \mathbf{0} & \mathbf{1} \\ -(\mathbf{V}^\dagger)^{-1} \mathbf{V} & -(\mathbf{V}^\dagger)^{-1} \mathbf{U} \end{pmatrix} \begin{pmatrix} \vec{u}_{n+1} \\ \vec{u}_n \end{pmatrix} \\ &= \mathbf{T} \begin{pmatrix} \vec{u}_{n+1} \\ \vec{u}_n \end{pmatrix}, \end{aligned} \quad (14)$$

giving

$$\begin{pmatrix} \vec{u}_1 \\ \vec{u}_0 \end{pmatrix} = \mathbf{T}^{N-1} \begin{pmatrix} \vec{u}_N \\ \vec{u}_{N-1} \end{pmatrix} = \begin{pmatrix} \mathbf{T}_{11} & \mathbf{T}_{12} \\ \mathbf{T}_{21} & \mathbf{T}_{22} \end{pmatrix} \begin{pmatrix} \vec{u}_N \\ \vec{u}_{N-1} \end{pmatrix}. \quad (15)$$

where \mathbf{T} is called the transfer matrix. We impose the boundary condition $\vec{u}_N = 0$, yielding

$$\vec{u}_1 = \mathbf{T}_{12} \vec{u}_{N-1} \quad \text{and} \quad \vec{u}_0 = \mathbf{T}_{22} \vec{u}_{N-1}. \quad (16)$$

Inserting into Eq. (11) allows to eliminate \vec{u}_{N-1} giving

$$\mathbf{\Phi} \vec{f} = (\mathbf{U}_0 \mathbf{T}_{22} + \mathbf{V} \mathbf{T}_{12}) \mathbf{T}_{22}^{-1} \quad (17)$$

the effective response of the surface layer to an external force \vec{f} under conditions of a fixed bottom boundary.

APPENDICES

3. Green's function transfer matrix formulation

The Green's function formulation starts from Eq. (8). Unlike the dynamical matrix, the Green's function is not sparse. We denote the individual elements as

$$\mathbf{G} = \begin{pmatrix} \mathbf{G}_{00} & \mathbf{G}_{01} & \mathbf{G}_{02} & \cdots & \mathbf{G}_{0N} \\ \mathbf{G}_{10} & \mathbf{G}_{11} & \mathbf{G}_{12} & \cdots & \mathbf{G}_{1N} \\ \mathbf{G}_{20} & \mathbf{G}_{21} & \mathbf{G}_{22} & \cdots & \mathbf{G}_{2N} \\ \vdots & \vdots & \vdots & \ddots & \vdots \\ \mathbf{G}_{N0} & \mathbf{G}_{N1} & \mathbf{G}_{N2} & \cdots & \mathbf{G}_{NN} \end{pmatrix} \quad (18)$$

and are now interested in extracting the surface Green's function, \mathbf{G}_{00} . Note that \mathbf{G}_{NN} and \mathbf{G}_{0N} can be determined equivalently.

From Eq. (8) we obtain generally $(N + 1)^2$ equations for our finite system with $N + 1$ layers. We will only pick the $N + 1$ equations involving the surface layer. Those are

$$\mathbf{U}_0 \mathbf{G}_{00} + \mathbf{V} \mathbf{G}_{10} = \mathbf{1} \quad (19)$$

$$\mathbf{V}^\dagger \mathbf{G}_{00} + \mathbf{U} \mathbf{G}_{10} + \mathbf{V} \mathbf{G}_{20} = \mathbf{0}$$

$$\mathbf{V}^\dagger \mathbf{G}_{10} + \mathbf{U} \mathbf{G}_{20} + \mathbf{V} \mathbf{G}_{30} = \mathbf{0}$$

$$\vdots$$

$$\mathbf{V}^\dagger \mathbf{G}_{n-1,0} + \mathbf{U} \mathbf{G}_{n,0} + \mathbf{V} \mathbf{G}_{n+1,0} = \mathbf{0} \quad (20)$$

$$\vdots$$

$$\mathbf{V}^\dagger \mathbf{G}_{N-1,0} + \mathbf{U}_N \mathbf{G}_{N,0} = \mathbf{0} \quad (21)$$

We now define the transfer matrix \mathbf{T}_n as

$$\mathbf{G}_{n+1,0} = \mathbf{T}_n \mathbf{G}_{n,0}. \quad (22)$$

The surface Green's function \mathbf{G}_{00} and stiffness Φ is then obtained from Eq. (19) as

$$\Phi = \mathbf{G}_{00}^{-1} = \mathbf{U}_0 + \mathbf{V} \mathbf{T}_0. \quad (23)$$

Combining Eqs. (20) and (22) yields

$$\mathbf{V} \mathbf{T}_n \mathbf{T}_{n-1} + \mathbf{U} \mathbf{T}_{n-1} + \mathbf{V}^\dagger = \mathbf{0} \quad (24)$$

from which we obtain

$$\mathbf{V} \mathbf{T}_{n-1} = -\mathbf{V} (\mathbf{U} + \mathbf{V} \mathbf{T}_n)^{-1} \mathbf{V}^\dagger. \quad (25)$$

APPENDICES

This continued fraction can be terminated by Eq. (21) which gives

$$\mathbf{V}\mathbf{T}_{N-1} = -\mathbf{V}\mathbf{U}_N^{-1}\mathbf{V}^\dagger. \quad (26)$$

Hence we can iterate Eq. (25) starting from Eq. (26) to obtain Φ from Eq. (23).

4. Renormalized dynamical matrices for long-ranged interactions

If the interatomic interaction acts over a distance of two layers, the dynamical matrix becomes

$$\mathbf{D} = \left(\begin{array}{cc|cc|cc|cc} \mathbf{U}_0 & \mathbf{V} & \mathbf{W} & 0 & 0 & 0 & 0 & \dots \\ \mathbf{V}^\dagger & \mathbf{U}_1 & \mathbf{V} & \mathbf{W} & 0 & 0 & 0 & \dots \\ \hline \mathbf{W}^\dagger & \mathbf{V}^\dagger & \mathbf{U} & \mathbf{V} & \mathbf{W} & 0 & 0 & \dots \\ 0 & \mathbf{W}^\dagger & \mathbf{V}^\dagger & \mathbf{U} & \mathbf{V} & \mathbf{W} & 0 & \dots \\ \hline 0 & 0 & \mathbf{W}^\dagger & \mathbf{V}^\dagger & \mathbf{U} & \mathbf{V} & \mathbf{W} & \dots \\ 0 & 0 & 0 & \mathbf{W}^\dagger & \mathbf{V}^\dagger & \mathbf{U} & \mathbf{V} & \dots \\ \hline 0 & 0 & 0 & 0 & \mathbf{W}^\dagger & \mathbf{V}^\dagger & \mathbf{U} & \dots \\ \vdots & \ddots \end{array} \right). \quad (27)$$

Hence we can renormalize the dynamical matrices \mathbf{U} and \mathbf{V} according to

$$\tilde{\mathbf{U}}_0 = \begin{pmatrix} \mathbf{U}_0 & \mathbf{V} \\ \mathbf{V}^\dagger & \mathbf{U}_1 \end{pmatrix}, \quad \tilde{\mathbf{U}} = \begin{pmatrix} \mathbf{U} & \mathbf{V} \\ \mathbf{V}^\dagger & \mathbf{U} \end{pmatrix} \quad \text{and} \quad \tilde{\mathbf{V}} = \begin{pmatrix} \mathbf{W} & 0 \\ \mathbf{V} & \mathbf{W} \end{pmatrix} \quad (28)$$

to yield an effective nearest layer model with more than three degrees of freedom per unit cell.

For interactions that extend over three neighboring layers we get

$$\mathbf{D} = \left(\begin{array}{ccc|ccc|cc} \mathbf{U}_0 & \mathbf{V} & \mathbf{W} & \mathbf{X} & 0 & 0 & 0 & \dots \\ \mathbf{V}^\dagger & \mathbf{U}_1 & \mathbf{V} & \mathbf{W} & \mathbf{X} & 0 & 0 & \dots \\ \mathbf{W}^\dagger & \mathbf{V}^\dagger & \mathbf{U}_2 & \mathbf{V} & \mathbf{W} & \mathbf{X} & 0 & \dots \\ \hline \mathbf{X}^\dagger & \mathbf{W}^\dagger & \mathbf{V}^\dagger & \mathbf{U} & \mathbf{V} & \mathbf{W} & \mathbf{X} & \dots \\ 0 & \mathbf{X}^\dagger & \mathbf{W}^\dagger & \mathbf{V}^\dagger & \mathbf{U} & \mathbf{V} & \mathbf{W} & \dots \\ 0 & 0 & \mathbf{X}^\dagger & \mathbf{W}^\dagger & \mathbf{V}^\dagger & \mathbf{U} & \mathbf{V} & \dots \\ \hline 0 & 0 & 0 & \mathbf{X}^\dagger & \mathbf{W}^\dagger & \mathbf{V}^\dagger & \mathbf{U} & \dots \\ \vdots & \ddots \end{array} \right), \quad (29)$$

APPENDICES

which leads to the renormalization

$$\tilde{\mathbf{U}}_0 = \begin{pmatrix} \mathbf{U}_0 & \mathbf{V} & \mathbf{W} \\ \mathbf{V}^\dagger & \mathbf{U}_1 & \mathbf{V} \\ \mathbf{W}^\dagger & \mathbf{V}^\dagger & \mathbf{U}_2 \end{pmatrix}, \quad \tilde{\mathbf{U}} = \begin{pmatrix} \mathbf{U} & \mathbf{V} & \mathbf{W} \\ \mathbf{V}^\dagger & \mathbf{U} & \mathbf{V} \\ \mathbf{W}^\dagger & \mathbf{V}^\dagger & \mathbf{U} \end{pmatrix} \quad \text{and} \quad \tilde{\mathbf{V}} = \begin{pmatrix} \mathbf{X} & 0 & 0 \\ \mathbf{W} & \mathbf{X} & 0 \\ \mathbf{V} & \mathbf{W} & \mathbf{X} \end{pmatrix}. \quad (30)$$

For interactions extending over even farther distances the procedure can be carried out accordingly.

5. Remarks

The displacement and Green's function transfer matrix formalisms of sections I A 2 and I A 3, respectively, give identical results. However, at the Brillouin zone boundary the motion of individual atoms decouples as the Einstein oscillator limit is reached. Hence we have $\mathbf{V} = 0$ and the transfer matrix \mathbf{T} as defined in Eq. (14) becomes singular. For practical purposes the Green's function formulation of section I A 3 is hence better suited and will be used in what follows.

Both algorithm are iterated exactly N times. Hence, the perpendicular dimension of the elastic half-space, i.e. the number of layers N , is explicitly included in the formulation. However, the quantity Φ is well defined in the limit of an infinite elastic half-space $N \rightarrow \infty$. Slowest convergence is obtained for the Γ point which converges to $\Phi(\Gamma) \rightarrow 0$ as $N \rightarrow \infty$. In this case, the half-space becomes infinitely compliant with respect to a uniform force.

B. Stiffness of the SC (100) and FCC (100) surfaces

We now use the Green's function transfer matrix formulation to compute the stiffness matrix for the simple cubic (SC) (100) and the face-centered cubic (FCC) (100) surfaces. The SC lattice is stabilized by nearest and next-nearest neighbor interactions, both with spring constants $k = 1$. This lattice is isotropic, and an analytical expression that agrees with our numerical results has been derived in Ref. 7. The FCC lattice interacts via nearest neighbors with spring constant $k = 1$ only.

For completeness, we compare the stiffness coefficients to the behavior of $\Phi(\vec{q})$ as expected for a continuum theory. The solution is obtained by a Fourier-transform of the Boussinesq

APPENDICES

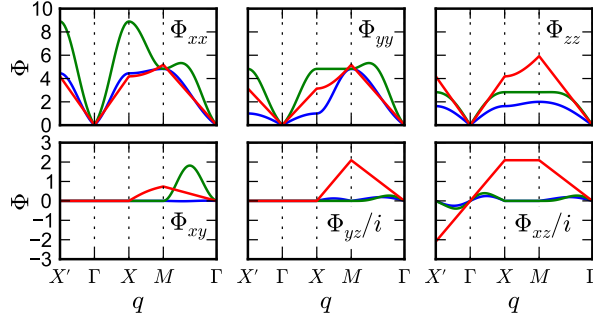


FIG. 1: Stiffness matrix coefficients for the FCC (100) (blue), the SC (100) (green) surface and an isotropic elastic solid (red).

solution for a concentrated point force on an isotropic elastic half-space [2], and reads

$$\mu \mathbf{G}(\vec{q}) = \begin{pmatrix} \frac{1}{q} - \frac{\nu q_x^2}{q^3} & -\frac{q_x q_y}{q^3} & -\frac{(1+2\nu)q_x}{2q^2} \\ -\frac{q_x q_y}{q^3} & \frac{1}{q} - \frac{\nu q_y^2}{q^3} & -\frac{(1+2\nu)q_y}{2q^2} \\ \frac{(1+2\nu)q_x}{2q^2} & \frac{(1+2\nu)q_y}{2q^2} & \frac{1-\nu}{q} \end{pmatrix}, \quad (31)$$

where μ is the shear modulus and ν Poisson's ratio. Figure 1 shows the value of the diagonal and off-diagonal components of the Φ matrix for the three models.

C. Elastic boundary conditions for atomistic calculations

While the linear elastic response of an atomic half-space is important to study contact mechanical problems in the linear response regime, such an approach can easily be used as an elastostatic boundary condition in molecular statics or dynamics simulations of for examples, indentation, crack propagation or nonlinear contact mechanics. The advantage of the scheme presented here over the fluctuation formulation of Campaña and Müser [8] is that the Green's function is obtained exactly for the interatomic potential under consideration hence minimizing mismatch of the elastic response at the interface. Furthermore, the response close to the Γ point is only poorly sampled by an evaluation using the fluctuation theorem, but becomes important in particular if the interaction in the atomistic part of the system reaches out beyond nearest neighbors and we need to compute the Green's function for multi-atom unit cells as discussed in section I A 4.

In order to properly couple an atomistic system with interactions that reach farther than nearest neighbors to the elastic half-space we need one final consideration. The surface

APPENDICES

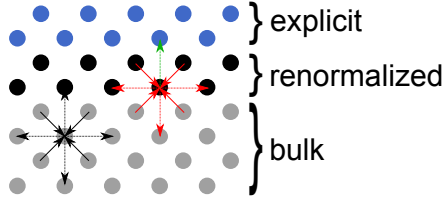


FIG. 2: For balance for renormalized surface with second-nearest neighbor interactions and explicit atoms on top.

stiffness Φ is based on the harmonic approximation in that the total energy of the system is expanded up to second order. In the bulk, first order terms cancel since the system is in equilibrium (see also Fig. 2). This does not hold for the surface, where terms linear in the displacements give rise to surface relaxation phenomena. Note that such relaxation cannot occur for crystals that interact via nearest-neighbors only, since in this case the nearest neighbor distance of the crystal equilibrium coincides with the minimum of the interaction potential and hence forces are zero. In particular when adding a layer of explicit atoms on top, the force due to these atoms needs to be cancelled on each renormalized atom.

The situation is depicted in Fig. 2. The green arrow shows the force that the explicit atom exerts on one of the renormalized atoms. In the bulk, this force would be cancelled by the red arrows, which are however missing in the elastic manifold. We hence need to enforce cancellation by adding a constant force of the same magnitude and opposite direction to the renormalized atom.

II. CONTACT MECHANICS OF ADHESIVE, RANDOMLY ROUGH SURFACES

The weak van-der-Waals interaction allows the Gecko to overcome gravity and stick to walls and ceilings [9–12]. The same force acts between everyday objects, and yet we are able to lift pens, plates, and almost anything else with ease. Fuller and Tabor resolved this adhesion paradox when finding that the apparent lack of macroscopic adhesion (or stickiness) is due to most surfaces' intrinsic roughness [13]. Yet, a detailed microscopic understanding of how the non-adhesive limit is controlled by the surface's geometry is lacking. In particular, it is unknown when a cross-over to sticky behavior happens, and how this cross-over depends on the statistical properties of the surface and the microscopic interaction. Here, we derive a

APPENDICES

simple scaling relation that describes the crossover from macroscopic non-adhesive to sticky behavior. This crossover is controlled by the characteristics of the rough surface on the smallest scale only. Such insights are important for the design of adhesives [9], but also to understand and prevent failure at interfaces, such as debonding of thin films and of composite materials [14], or fretting and pitting in tribological systems.

The microscopic origins of adhesion are manifold and range from simple intermolecular interactions [15] over capillary bridges [16] and adhesive films [17] to the influence of bubbles of air at the contact [18]. Microscale adhesion is characterized by the energy per surface area γ that is gained when two nominally flat surfaces are brought into contact. Such interactions give rise to macroscale adhesion, or stickiness, that manifests itself in nonzero pulloff forces for the contacting surfaces.

Cohesive or Dugdale zone models are used to capture the effect of the adhesive energy γ in continuum theories [19]. An important example is the Maugis-Dugdale (MD) model of the adhesion of a sphere on an elastic substrate [20] that has been extensively used to interpret scanning probe adhesion experiments [21]. Many real surfaces are not flat as assumed in continuum theories. Roughness at the atomic length scale can have appreciable influence on contact and adhesion of objects as simple as spherical tips with atomic scale diameters [3, 22]. The roughness on macroscopic surfaces typically extends over many length scales and is suitably approximated by Gaussian self-affine fractals where the root mean square height fluctuation δh between two points at distance λ on the surface scales as $\delta h \sim \lambda^H$ for λ between λ_s and λ_L [23]. We here investigate the adhesion of such surfaces that are held rigid on a square flat deformable ideally elastic substrate for wide variations in Hurst exponent H , root mean square slope h'_0 , small wavelength cutoffs λ_s , and large wavelength cutoff λ_L . For the interaction between rigid surface and elastic substrate we choose a Lennard-Jones type potential as an approximation for the van-der-Waals interaction (see methods). The sites on the elastic substrate are arranged on a square grid with lattice constant a_0 and will be regarded as atoms.

The elastic interaction is solved using a Fourier-transform technique [8] with a linearized surface Green's function. We only treat displacements in z -direction normal to the surface such that the total elastic energy is given by $E_{\text{el}} = \frac{A_0}{4} \sum_q q E^* u_z^2(\vec{q})$ where A_0 is the total area of the elastic half space and \vec{q} is a reciprocal space vector in the plane of the half space. This corresponds to the isotropic elastic stiffness matrix Eq. (31) with only a single degree

APPENDICES

of freedom. Each discrete point on the elastic manifold will be regarded as an “atom”. Each atom occupies unit area, and interacts with the rigid surface through the potential $V(x, y, z) = v(z - h(x, y))$ where $h(x, y)$ is the rough surface. For the interaction of two flat surfaces, the adhesive energy w per unit area is given by the minimum of the atomic interaction $v(z)$. Rigid Gaussian random surfaces with Hurst exponents H and rms slopes $h'_0 = \sqrt{\langle |\nabla h|^2 \rangle}$ were generated using a Fourier-filtering algorithm. All wavevectors with $q > 2\pi/\lambda_s$ have zero power.

After finding the equilibrium contact geometries for different external loads, we partition the sites on the elastic surface into regions of atoms that feel a repulsive and regions that feel an attractive force, as well as regions that do not interact. Fig. 3a shows these individual regions at a fractional repulsive area of 5%. Let us first characterize the geometry of the repulsive patches by determining the length P of their perimeter. First, we note that $P_{\text{rep}} \sim A_{\text{rep}}$ in stark contrast to the slit island analysis which yields $P \sim A^{-H}$ [23]. The latter is a consequence of the fact that the area of the island has dimension 2 while the perimeter (or “coastline”) has dimension $2 - H$. This implies that for the elastic contact problem the total repulsive patch is a fractal object. To find the length scale that controls A/P consider the distribution $p(w)$ of the lengths w of segments that are obtained from one-dimensional slices through the repulsive contact geometry (see Fig. 3b). The total repulsive area is then given by $A_{\text{rep}} = a_0 \int dw w p(w) = a_0 \bar{w}$, and each segment contributes $2a_0$ to the perimeter, hence $P_{\text{rep}}/A_{\text{rep}} = \alpha/\bar{w}$ with $\alpha = 2$. Numerically, we find a slightly different value of $\alpha \approx 2.8$ which is attributable to segments of the perimeter that area parallel to the w -segments missing from the total estimate. This is an effect of the discrete character of the contact patches.

Remarkably, we find that the length \bar{w} only weakly depends on the contact area and adhesion strength (see Fig. 3c). This observation holds for all surfaces studied here. Although the contacting surface has roughness on all lengths, only a single length scale \bar{w} that is of the order of the short cutoff λ_s appears to be important for a description of the contact problem.

Besides giving the ratio between area and circumference, the length \bar{w} plays the role of a contact diameter. From continuum considerations, it is straightforward to show that the air gap Δ between the two separating surfaces raises asymptotically as $\Delta = g(R) \sim R^{\frac{3}{2}}$ for small distances R from the contact edge. Numerically, we find exactly this power-law

APPENDICES

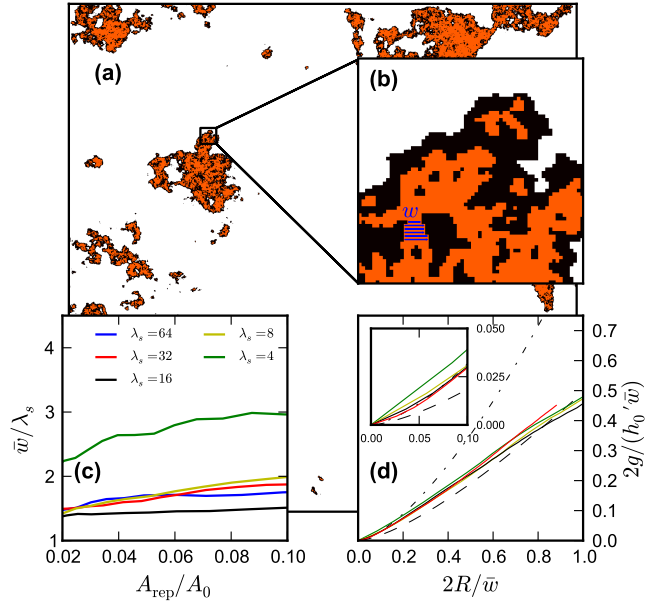


FIG. 3: (a) Map of the contacting atoms that feel a repulsive (orange) and attractive (black) force when a rough surface is pushed against a flat elastic manifold (the surface shown has $H = 0.8$, $h'_0 = 0.1$, $\lambda_s = 4$ and $\lambda_L = 2048$). Atoms that feel a repulsive force cover an area of roughly 5%. (b) Zoom into a 64×64 region of that surface. The blue vertical lines show individual segments of length w (see text). (c) Dependence of the average segment length \bar{w} on contact area. (d) Shape of the gap between rigid and elastic surfaces g as we move away from the edge of the contact patch in the non-adhesive hard-wall limit. The inset shows the behavior for $R < 0.05\bar{w}$ close to the contact edge. The dashed line is the gap obtained for a 2D wedge indenter, and the dashed-dotted line shows a $3/2$ power law.

behavior for the rough contact for small distances from the contact edge with a crossover to linear behavior at larger distances. Indeed, the gap data collapses as we normalize all distances by the contact radius $\bar{w}/2$ and all heights by $h'_0\bar{w}/2$ as shown in Fig. 3d.

The partitioning into repulsive and attractive regions of the area $A = A_{\text{rep}} + A_{\text{att}}$ entails an identical partitioning of the total load $N = N_{\text{rep}} - N_{\text{att}}$. We find that the repulsive load N_{rep} shows a linear Amontons-like dependence on the repulsive area A_{rep} which follows the same law $\kappa N_{\text{rep}} = h'_0 E^* A_{\text{rep}}$ that was found for nonadhesive contact [4, 24] with a similar value of $\kappa \approx 2$. Additionally, the attractive load is given by the average force γ/Δ_c times the attractive area, where Δ_c is the range at which the potential energy drops to zero. Hence

APPENDICES

we have

$$N = \frac{h'_0 E^*}{\kappa} A_{\text{rep}} - \frac{\gamma}{\Delta_c} A_{\text{att}} \quad (32)$$

for the total load N .

We now relate the attractive area A_{att} to the repulsive area A_{rep} . In what follows, we assume that the adhesive interaction only weakly perturbs the shape of the gap such that we can use the 3/2 power-law separation to estimate the attractive area. Independent of the exact functional form of the separation of the contact lips $g(R)$, roughly all sites within $R = g^{-1}(\Delta_c)$ around the repulsive clusters constitute the area A_{att} . For small \bar{w} , large Δ_c and small h'_0 this will lead to mutually overlapping regions. If on the other hand $\bar{w} \gg R$ then the attractive region will be small compared to the cluster size and we expect $A_{\text{att}} \approx PR$. We hence estimate the attractive area to be

$$\frac{A_{\text{att}}}{A_{\text{rep}}} \sim \left(\frac{2\Delta_c}{h'_0 \bar{w}} \right)^{\frac{2}{3}}, \quad (33)$$

with a constant of proportionality β that is of order 1.6. Fig. 4 shows the value of β as obtained from the numerical calculations. As λ_s increases the value of β converges towards roughly unity. For small λ_s we expect deviations from the ideal behavior since \bar{w} becomes of order of the Δ_c/h'_0 .

The value of β is remarkably independent of the interaction strength γ . Fig. 5a shows the dependence of this factor for value of γ ranging from zero to 0.1. For $\lambda_s = 16$ and $\lambda_s = 32$ this value remains constant at roughly 1.6. The ratio of $N_{\text{att}}/A_{\text{att}}$, however, starts to deviate from the average force γ/Δ_c over the range of adhesive energies shown. This is most likely attributable to a deviation from the 3/2 power law behavior of the air gap due to the influence of the adhesive interaction.

We now have an approximate expression for the total load N as a function of the the repulsive (contact) area A_{rep} . Hence, we can define a renormalized κ' by

$$\frac{1}{\kappa'} = \frac{N}{h'_0 E^* A_{\text{rep}}} = \frac{1}{\kappa} - \frac{\beta \gamma}{h'_0 E^* \Delta_c} \left(\frac{2\Delta_c}{h'_0 \bar{w}} \right)^{\frac{2}{3}} \quad (34)$$

that depends explicitly on the adhesive energy γ , the interaction range Δ_c of the interatomic potential, the root mean square slope h'_0 as well as the internal length scale \bar{w} . Hence, the influence of adhesion is controlled by the short wavelength of the rough surface only.

The renormalized κ' can be again formally split into a repulsive and an attractive contribution. Fig. 6 shows the dependence of these individual contributions on \bar{w} . Here, the

APPENDICES

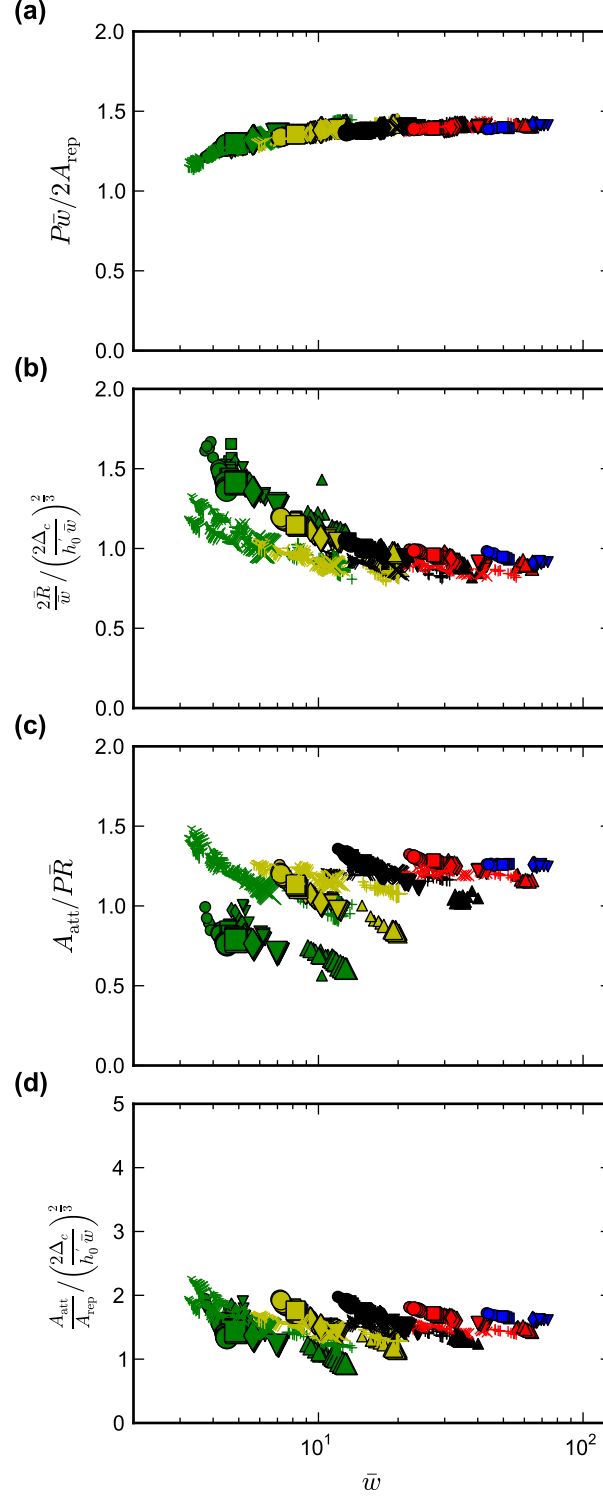


FIG. 4: (a) Relationship of perimeter P , \bar{w} and repulsive area A_{rep} (b) Behavior of the width \bar{R} is the attractive area as a function of \bar{w} . Here \bar{R} is the average R over the whole contact geometry. (c) Relationship of the attractive area A_{att} to perimeter P and the average width \bar{R} . (d) Scaling of $A_{\text{att}}/A_{\text{rep}}$. This plot is the product of (a), (b) and (c). In all plots, symbols denote surfaces with different Hurst exponents H and root mean square slopes h'_0 , while color denotes the short wavelength cutoff λ_s . Symbol size is a measure of λ_L/λ_s where only data with $\lambda_L/\lambda_s \geq 128$ is shown.

APPENDICES

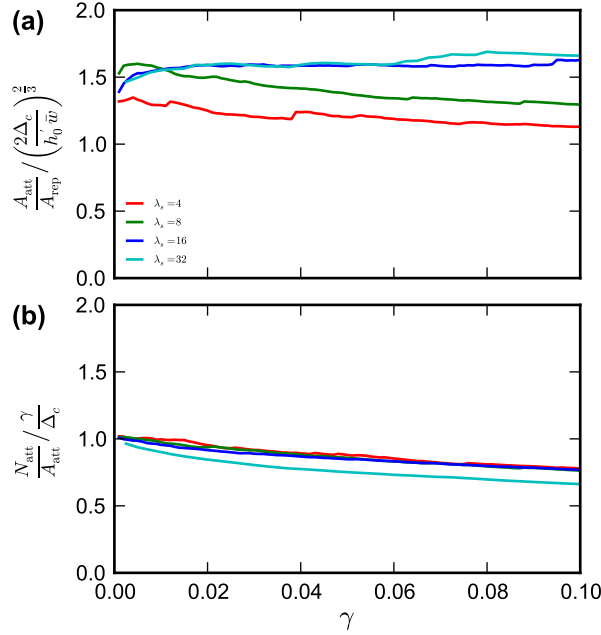


FIG. 5: (a) Dependence of the ratio of attractive to repulsive area as a function of the strength of the adhesive interaction γ . (b) Dependence of the ratio of attractive load to attractive area on γ . For larger γ , this ratio starts to deviate from the average force γ/Δ_c .

attractive κ in Fig. 6a nicely follows the relationship Eq. (34). The repulsive κ (Fig. 6b) is close to a κ obtained from a fully nonadhesive calculation (Fig. 6c).

Equation (34) now allows to determine the onset of the macroscopic adhesive behavior, i.e. non-zero pulloff forces for the two surfaces. Such a condition is obtained when $N < 0$ and hence $1/\kappa' < 0$. From this condition we get

$$\bar{w} < 2\Delta_c \frac{(\kappa\beta)^{3/2}}{(h'_0)^{5/2}} \left(\frac{\delta}{\Delta_c} \right)^{3/2}, \quad (35)$$

as the upper bound on the admissible values of \bar{w} . Since $\bar{w} \approx \lambda_s$ macroscopic adhesive behavior can only be obtained if the roughness extends down the length scale given by Eq. (35). Equation (35) clarifies the result of Fuller and Tabor [13] that roughness can destroy adhesive interaction.

From this scaling relation we can also obtain a criterion for when macroscopic adhesive behavior can be ruled out. The value $\bar{w} = 1$ is a natural lower bound since roughness cannot extend below the atomic scale. Then we find

$$\delta > \frac{a_0}{2^{2/3}} \frac{(h'_0)^{5/3}}{\kappa\beta} \left(\frac{\Delta_c}{a_0} \right)^{1/3} \quad (36)$$

APPENDICES

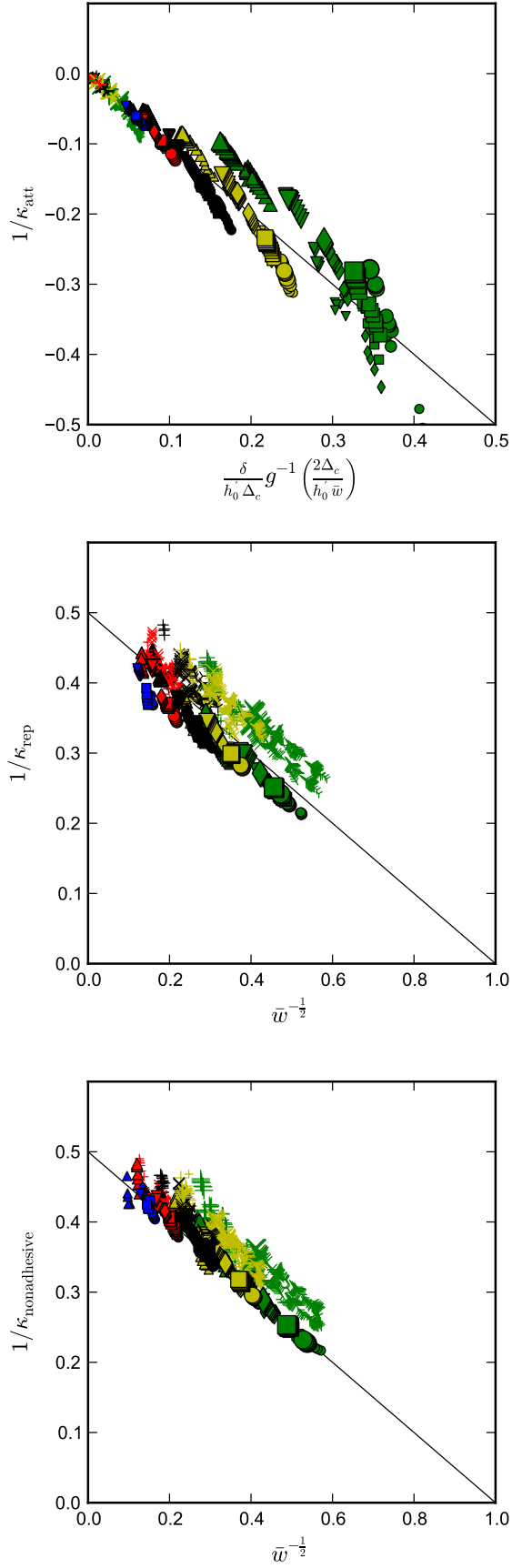


FIG. 6: (a) Attractive κ . (b) Repulsive κ . (c) κ obtained from a nonadhesive calculation (i.e. for $\gamma = 0$).

APPENDICES

for surfaces to become adhesive. All dimensionless quantities in Eq. (36) are on the order of unity, giving roughly $\delta/a_0 > (h'_0)^{\frac{5}{3}}$.

-
- [1] H. Hertz, *J. reine angew. Math.* **92**, 156 (1881).
 - [2] K. L. Johnson, *Contact Mechanics* (Cambridge University Press, 1985).
 - [3] B. Luan and M. O. Robbins, *Nature* **435**, 929 (2005).
 - [4] S. Akarapu, T. Sharp, and M. O. Robbins, *Phys. Rev. Lett.* **106**, 204301 (2011).
 - [5] L. M. Falicov and F. Ynduráin, *J. Phys. C: Solid State Phys.* **8**, 147 (1975).
 - [6] V. R. Velasco and F. Ynduráin, *Surf. Sci.* **85**, 107 (1979).
 - [7] Y. Saito, *J. Phys. Soc. Jpn.* **73**, 1816 (2004).
 - [8] C. Campaña and M. H. Müser, *Phys. Rev. B* **74**, 075420 (2006).
 - [9] C. Creton and S. N. Gorb, *MRS Bulletin* **32**, 466 (2007).
 - [10] K. Autumn, M. Sitti, Y. A. Liang, A. M. Peattie, W. R. Hansen, S. Sponberg, T. W. Kenny, R. Fearing, J. N. Israelachvili, and R. J. Full, *Proc. Natl. Acad. Sci. USA* **99**, 12252 (2002).
 - [11] K. Autumn, Y. A. Liang, S. T. Hsieh, W. Zesch, W. P. Chan, T. W. Kenny, R. Fearing, and R. J. Full, *Nature* **405**, 681 (2000).
 - [12] P. F. A. Maderson, *Nature* **203**, 780 (1964).
 - [13] K. N. G. Fuller and D. Tabor, *Proc. R. Soc. Lond. A* **345**, 327 (1975).
 - [14] M. Lane, *Annual Review of Materials Research* **33**, 29 (2003).
 - [15] J. N. Israelachvili, *Intermolecular and Surface Forces* (Academic Press, London, 1991).
 - [16] G. Huber, H. Mantz, R. Spolenak, K. Mecke, K. Jacobs, S. N. Gorb, and E. Arzt, *Proc. Natl. Acad. Sci. USA* **102**, 16293 (2005).
 - [17] A. R. C. Baljon and M. O. Robbins, *Science* **271**, 482 (1996).
 - [18] C. Gay and L. Leibler, *Phys. Rev. Lett.* **82**, 936 (1999).
 - [19] D. S. Dugdale, *J. Mech. Phys. Solids* **8**, 100 (1960).
 - [20] D. Maugis, *J. Colloid Interf. Sci.* **150**, 243 (1992).
 - [21] B. Gotsmann and M. A. Lantz, *Phys. Rev. Lett.* **101**, 125501 (2008).
 - [22] B. Luan and M. O. Robbins, *Phys. Rev. E* **74**, 26111 (2006).
 - [23] B. B. Mandelbrot, *The Fractal Geometry of Nature* (W. H. Freeman, 1982).
 - [24] S. Hyun, L. Pei, J. Molinari, and M. O. Robbins, *Phys. Rev. E* **70**, 26117 (2004).